Original Research

Radiogenomic landscape: Assessment of specific phagocytosis regulators in lower-grade gliomas

Aierpati Maimaiti[1*], Aimitaji Abulaiti[1*], Bin Tang[2*], Yilidanna Dilixiati[3], Xueqi Li[2], Suobinuer Yakufu[2], Yongxin Wang[1], Lei Jiang[1] and Hua Shao[2]

[1]Department of Neurosurgery, Neurosurgery Centre, The First Affiliated Hospital of Xinjiang Medical University, Urumqi 830054, China; [2]Imaging Center, The First Affiliated Hospital of Xinjiang Medical University, Urumqi 830054, China; [3]Xinjiang Medical University, Urumqi 830054, China
*These authors contributed equally to this paper.
Corresponding authors: Lei Jiang. Email: jiangleidr@126.com; Hua Shao. Email: 383283715@qq.com

Impact Statement

Genome-wide CRISPR-cas9 knockout screens have emerged as an outstanding approach to characterize tumor growth driver genes. This study aimed to investigate the core genes linked to lower-grade glioma (LGG)-specific phagocytosis regulators (PRs) using the CRISPR-cas9 screening database DepMap, which could lead to new targets for LGG therapy and serve as the basis for developing a non-invasive radiogenomics approach to assess LGG patients' survival outcomes and treatment response.

Abstract

Genome-wide CRISPR-Cas9 knockout screens have emerged as a powerful method for identifying key genes driving tumor growth. The aim of this study was to explore the phagocytosis regulators (PRs) specifically associated with lower-grade glioma (LGG) using the CRISPR-Cas9 screening database. Identifying these core PRs could lead to novel therapeutic targets and pave the way for a non-invasive radiogenomics approach to assess LGG patients' prognosis and treatment response. We selected 24 PRs that were overexpressed and lethal in LGG for analysis. The identified PR subtypes (PRsClusters, geneClusters, and PRs-score models) effectively predicted clinical outcomes in LGG patients. Immune response markers, such as CTLA4, were found to be significantly associated with PR-score. Nine radiogenomics models using various machine learning classifiers were constructed to uncover survival risk. The area under the curve (AUC) values for these models in the test and training datasets were 0.686 and 0.868, respectively. The CRISPR-Cas9 screen identified novel prognostic radiogenomics biomarkers that correlated well with the expression status of specific PR-related genes in LGG patients. These biomarkers successfully stratified patient survival outcomes and treatment response using The Cancer Genome Atlas (TCGA) database. This study has important implications for the development of precise clinical treatment strategies and holds promise for more accurate therapeutic approaches for LGG patients in the future.

Keywords: CRISPR-cas9, lower-grade glioma, radiogenomics, phagocytosis regulators, prognostic

***Experimental Biology and Medicine* 2023; 248: 2289–2303. DOI: 10.1177/15353702231211939**

Introduction

Lower-grade gliomas (LGGs) represent around 43.2% of central nervous system (CNS) gliomas, with 6500–8000 new cases diagnosed annually in the USA.[1,2] LGG is a heterogeneous group of neuroepithelial tumors resulting from the malignant transformation of oligodendrocytes or astrocytes,[3] which includes glioma tumors of World Health Organization (WHO) grade III (intermediate grade) and grade II (diffuse lower grade). Although LGG patients have a better clinical prognosis than grade IV tumors, their survival duration ranges from 1 to 15 years,[4] following surgical excision, followed by radiation and chemotherapy. In addition, 70% of LGG patients develop high-grade gliomas or relapse and die within 10 years.[5] Therefore, identifying new glioma biomarkers may result in new information about risk and prognosis.

Most regulators of macrophage phagocytosis undergo a high enrichment in immunological responses, inflammatory disorders, and macrophage phagocytosis. It has been used recently in several studies. Immunohistochemistry (IHC), mesenchymal scoring, and cell density were used to evaluate inflammatory cell density and mesenchymal infiltration in tumor tissue.[6] In many types of cancer, they have been linked to poor clinical outcomes.[7] Macrophages are involved in tissue remodeling, immunity, and local and systemic inflammation. They carry out several functions,

including antigen presentation, microbial cytotoxic defense, cytokine and complement components secretion, and phagocytosis.[8] Tumor-associated macrophages (TAMs) are critical for tumor progression and metastasis in the tumor microenvironment. It is widely present in a variety of tumors.[9] They are integrally engaged in immunosuppression, angiogenesis, and profibrotic activities in malignant and normal tissues.[10] TAM may promote tumor progression, infiltration, metastasis, and drug resistance.[11] The protumor effects of TAM on tumor initiation, metastasis, angiogenesis, antitumor immunosuppression, and treatment resistance have been studied.[12] Macrophages have two polarization activation stages, according to conventional concepts: the classical activation phase (M1, produced by lipopolysaccharide and interferon [IFN]) and the replacement activation phase (M2, induced by IL-13 or IL-4).[13] As per the results of earlier studies, TAM possesses an M2-like phenotype that suppresses the immune system and promotes tumor growth.[14] Depleting M2-like TAMs or causing them to change their phenotype to that of M1-like TAMs might therefore directly increase their cytotoxicity. Indirect cytotoxic T cell activation to kill tumor cells is one potential antitumor immunotherapeutic approach.[15,16] Several action mechanisms of TAM in tumor immunosuppression have been elucidated, and recent clinical studies of possible therapeutic agents targeting the aforementioned novel targets have been conducted.[17,18] In addition, some recent research has focused on phagocytosis, a critical activity of macrophages, and the reactivation of antitumor immunity through the CD24/Siglec-1075, CD47/SIRP, and PD-1/PD-L1 pathways. Each of the following strategies will be effective, thereby bringing cancer immunotherapy to the forefront of research.

Recent advances in genetics have enabled extensive genomic and transcriptomic investigations to identify the underlying molecular mechanisms of cancer. Radiology is another new technology that can identify important imaging features that cannot be captured by any other method and use the capabilities of digital imaging. Radiology can transform biological images into quantifiable variables that may then be analyzed to increase the efficacy of preoperative expectations, tumor categorization, prognosis prediction, and therapy response.[19] Radiogenomics is a new interdisciplinary research that combines radiology and genomics. It is the most fundamental way for retrieving sophisticated genomic information. It has recently been developed to link radiology to wider biological characteristics, including proteomics and metabolomics.[20] Previous research has used non-invasive digital imaging characteristics to investigate tumor mutation burden, tumor gene expression, methylation patterns, and subtypes.[21–23] Furthermore, the integration of radiology and genomics has aided in the improvement of clinical prediction efficiency in certain cancers.[24,25] Therefore, radiogenomics may aid in comprehending the molecular characteristics of distinct malignancies and enable real-time monitoring for specific patient clinical care.

Clustered conventional interspatial short palindromic repeat-associated protein 9 (CRISPR/Cas9) is a newly discovered and developed gene-editing method.[26] In this method, a single-guide RNA (sgRNA) guides the Cas9 endonuclease precisely to the target site, where it causes a DNA double-strand break and site-specific genomic changes. Compared to conventional gene-editing techniques, such as transcription activator-like effector nucleases and zinc finger nucleases, CRISPR/Cas9-mediated gene editing is more adaptable, effective, and accurate.[27] CRISPR/Cas9 technology has been intensively investigated since its first use in mammalian cells in 2013,[28,29] and its applications have moved beyond gene editing in cells to biology.[30] One of the hottest topics in cancer-treatment schemes is CRISPR/Cas9 due to its potential use in gene-related therapy. Several CRISPR/Cas9-mediated cancer therapeutic approaches have been developed for many cancer types, including tumor immunotherapy, tumor research modeling, tumor-associated gene manipulation, and anticancer drug resistance overcoming.[31] By employing CRISPR/Cas9, researchers can selectively target and modify specific genes involved in these processes to better understand their functional significance. For instance, the loss or mutation of certain tumor suppressor genes, such as TP53 or PTEN, has been associated with poor prognosis in LGG patients. Cas9's ability to bind to specific DNA locations via directing RNA and protospacer adjacent motif (PAM) is a critical characteristic. Thus, a catalytically dead Cas9 (dCas9) without endonuclease activity may be linked to transcriptional activators and repressors to regulate gene expression throughout the genome. CRISPR interference (CRISPRi) is a kind of transcriptional suppression relying on dCas9. When dCas9 is co-expressed with sgRNA, it hinders the regulation of transcription start complexes and transcriptional expansions. CRISPRi can not only successfully inhibit the expression of numerous target genes in *Escherichia coli* at the same time but its effects are also reversible and do not seem to spread beyond the target.[32] CRISPR activation, however, uses dCas9 linked to an activation effector for the purpose of recruiting RNA polymerase and transcriptional machinery to trigger the target gene's expression.[33] The CRISPR system, by modifying the sgRNA sequence, provides an editable DNA-binding platform for recruiting appropriate proteins to the target DNA sequence, exposing the tool's ability to precisely regulate gene expression.[34]

Therefore, the establishment of a novel non-invasive technique is of utmost importance for aiding clinicians in making informed decisions while reducing unnecessary invasive tests. This study sought to develop a non-invasive radiomics technique capable of identifying macrophage phagocytosis regulator (PR) signatures and predicting survival outcomes in patients with LGG. Genomic data from 481 LGG cases were collected and subsequently analyzed by integrating a previously reported CRISPR-Cas9 screen focused on regulators of cancer cell phagocytosis. In addition, the study combined differentially expressed genes (DEGs) between LGG tissue and normal tissue in The Cancer Genome Atlas (TCGA) and the CRISPR-Cas9 screen for $|\mathrm{CERES}| > 0.5$ on genes vital for the proliferation and survival of LGG cell lines. This integration aimed to identify specific lethal and overexpressed PRs in LGG. In our final genomic investigation, we successfully identified genes that serve as predictive markers for PRs. Furthermore, we developed a PRs-score system that uses gene expression levels to evaluate the PRs status of samples. Regarding radiomics, we acquired 120 complete digital image samples from The Cancer Imaging

Archive (TCIA) database. Following the extraction of image characteristics using radiomics, we employed the PRs-score system classification to construct image prediction models.

Materials and methods

Identification of LGG-specific PRs

Regulators of cancer cell phagocytosis were identified by conducting CRISPR-Cas9 screens on a set of 730 genes described in previous study.[35] The CRISPR-Cas9 methodology allowed for the precise targeting and manipulation of genes. The CERES computational method,[36] which accounts for copy number specificity effects, was used to estimate gene-dependent levels from the CRISPR-Cas9 screens. To do this, the Cancer Cell Line Encyclopedia (CCLE) database was searched to retrieve gene mutation, copy number, and expression data from 16 primary non-metastatic LGG cell lines. The CERES package was used to analyze input files obtained from the DepMap database, providing insights into the genes essential for proliferation and survival in each LGG cell line. Genes with negative scores indicated that knocking out these genes inhibited cell line survival, while genes with positive scores suggested that knocking them out promoted cell line survival and proliferation. A threshold of $|\text{CERES}| > 0.5$ was applied to include all genes for further analysis. Differential analysis was performed on 491 LGG specimens from the TCGA database and 103 normal cortical specimens from the Genotype-Tissue Expression (GTEx) project. Using screening thresholds of $|\text{logFC}| > 1$ and $|\text{adj. } P \text{ value}| < 0.05$, DEGs were identified. These DEGs represented genes that exhibited significant differences in expression between LGG and normal cortical tissues. Overall, the identified genes from the three steps described above were then intersected to determine specific PRs in LGG. These PRs are genes that play a role in the regulation of cancer cell phagocytosis and were found to be essential for survival, proliferation, and exhibited differential expression in LGG compared to normal cortical tissues.

Transcriptome data preprocessing

After excluding non-coding RNAs, RNA-Seq data from TCGA database–contained 491 LGG samples with WHO classifications II–III (Level-3 HTseq-FPKM) and RNA-Seq data from the GTEx project's 103 normal cortical samples were used as normal sample controls for conducting the differential analysis. Furthermore, 481 samples were excluded from subsequent modeling due to the following reasons: repeat sequencing, total survival time < 1 day, unclear WHO classification, no survival status, and non-primary LGG. With the aid of the caret package, the TCGA-LGG database–contained 481 samples were randomly classified in a 7:3 ratio; TCGA-LGG-1 served as the modeling cohort, and TCGA-LGG-2 served as the internal validation cohort. In the meantime, the GPL570 platform–based GSE16011 dataset was retrieved from the Gene Expression Omnibus (GEO) database, and 80 of these LGG patients with WHO classifications II–III were maintained as the external validation cohort (GEO-LGG). In addition, as the external validation group, we downloaded the CGGA-693 project (CGGA-LGG-1, 332 patients) and the CGGA-325 project (CGGA-LGG-2, 162 patients), both of which had the complete survival data of LGG patients. Finally, we used the TCGA-LGG-1 and TCGA-LGG-2 cohorts as well as the GEO-LGG, CGGA-LGG-1, and CGGA-LGG-2 cohorts for modeling, internal validation, and external validation. Notably, we used the sva package to conduct background correction, normalization, and expression calculation for the genes included in modeling to guarantee validation comparability while undertaking internal and external validation.

Enrichment analysis and clustering algorithms

For the annotation of biological processes, cellular components, and molecular functions of genes, we used the Gene Ontology (GO) database. Using the Kyoto Encyclopedia of Genes and Genomes (KEGG) database, gene pathways were annotated. The clusterProfiler package was used to conduct GO and KEGG analyses. Significant enrichment pathways were defined as per the following criteria: P values < 0.05 and q value < 0.05. Using the ConsensusClusterPlus package in 1000 iterations to achieve accurate classification, an unsupervised clustering analysis was carried out to discover various patterns according to gene expression. In addition, using the NMF package in the R software, all TCGA-LGG cohort's patients were divided into three sub-consensus groups depending on certain PRs' expression levels.

Construction of the PRs scoring system

Patients from the TCGA-LGG cohort were divided at random (in a ratio of 7:3) into a dataset for internal training and another for internal validation. To eliminate highly linked genes, risk models were developed using the Least Absolute Shrinkage and Selection Operator (LASSO) model. Gene expression values were integrated with LASSO-Cox coefficient weights to construct risk score equations. The risk scores' prognostic significance throughout the whole dataset and the external validation dataset was evaluated by means of univariate and multivariate Cox regression analyses. The predictive accuracy between the risk score and traditional clinicopathological indicators was compared using time-dependent receiver operating characteristic (tROC) curves. The area under the curve (AUC) and ROC curves were generated using the survivalROC package.

Pan-cancer analysis of signature genes

Using differential expression analysis between tumors and nearby normal tissue for each cancer type, we first looked at alterations in gene expression patterns for signature genes ($|\log2(\text{FC})| > 1.5$, FDR 0.05). We used clinical data from tumor samples from 33 different cancers, with some uncensored data being excluded, to derive the survival landscape of signature genes from TCGA analysis of the correlation between gene expression and patients' survival. Samples with competing risks of cancer death were filtered out (for disease specific survival (DSS) and disease free interval (DFI) data). According to the mRNA expression and clinical survival data that were combined by sample barcode, tumor samples were divided into low- and high-expression groups

using median mRNA values. Then, we fitted survival times and survival status within the two groups with the aid of the R package SURVIVAL. For each gene for each cancer, Logrank tests and Cox proportional hazards models were conducted. Next, we also retrieved 10,234 samples from 33 cancers with single nucleotide variant (SNV) data from the TCGA database. Seven mutation types were included in this study, including In_Frame_Del, Nonsense_Mutation, Missense_Mutation, In_Frame_Ins, Splice_Site, and Frame_Shift_Ins. Using percentage heat maps, mutation frequencies for pan-cancer were summarized. In addition, 11,495 samples' copy number variation (CNV) data in the TCGA database were examined to identify the cases of significantly altered CNV amplification or deletion in the patient group. The copy number alterations of each gene were enhanced by the heterozygosity and purity of amplifications and deletions, of which more than 5% were considered high-frequency CNVs. Conversely, we annotated each gene promoter's methylation probes. Each gene's methylation was compared between tumor and normal samples using the Wilcoxon signed-rank test. Using a P value cut-off of 0.05, significantly hypo- or hypermethylated genes were discovered. Finally, 7876 TCGA database samples representing 32 cancer types had their pathway activity scores estimated using the Reverse Phase Protein Array (RPPA) data from the cancer protein atlas (TCPA) database. The pathways addressed are PI3K/AKT, TSC/mTOR, hormone AR, RAS/MAPK, RTK, DNA damage response, hormone ER, apoptosis, EMT, and cell cycle pathways. All of these are recognized cancer-related pathways.[37]

Immunological correlation analysis

To determine the immunological features of LGG samples, the single-sample gene set enrichment analysis (ssGSEA) algorithm was applied. Immune checkpoints have a role in the inhibition of lymphocyte activation and evasion of immune surveillance of cancer. We analyzed 14 immune checkpoint gene expression, including CTLA4 and PD-1 in low- and high-risk groups to determine whether immune checkpoints are involved in the precancerous activity. Then, with the aid of the Cmap tool (https://clue.io/), we examined the action mechanism (MoA) of potential compounds that were screened targeting PR properties.

Identification of radiomic features from MRI

Using MRIcron software, 120 patients matching the TCGA-LGG cohort's MRI images were obtained from the TCIA database and converted from DICOM to NIFTI formats for further analysis.[38] After mapping the region of interest (ROI) and registering FLAIR, T2W, and T1CE to the T1W images following the processing protocol of previous literature, brain tissue was acquired for the FLAIR, T2W, and T1ce images using the T1W brain regions as masks.[39] Subsequently, image features were extracted using PyRadiomics.[40] After feature extraction, we applied several downscaling and machine learning techniques to develop imaging genomics models. The best AUC values in the test set were used as selection criteria to determine the optimal technique for developing the final model. In particular, the data were normalized using the Z-Score and Minmax normalization methods; the characteristics were preprocessed using principal component analysis (PCA) and Pearson correlation coefficient (PCC) methods; the most effective features were selected using analysis of variance (ANOVA), Kruskal–Wallis (KW), and recursive feature elimination (RFE). Radiogenomics classifier models were developed using several machine learning classifiers, including logistic regression, AdaBoost, LR-Lasso, random forest, plain Bayes, linear discriminant analysis (LDA), and support vector machine (SVM). A total of 9504 models were created, with one being chosen as the best model. In addition, ROC curve analysis, which computed AUC values using 1000 replicate samples, was used to evaluate the performance of the model. With the aid of Python (3.7.6)-based FeAture Explorer Pro (FAEPro, V 0.3.7), the aforementioned feature selection procedure was carried out.[41]

Results

Identification of specific PRs in LGG

When monoclonal antibodies are used to treat tumor antigens, the majority of cancer cells are phagocytosed by macrophages, and CRISPR techniques have helped to identify the key regulators that prevent antibody-dependent cell phagocytosis (ADCP).[35] Therefore, to identify particular PRs in LGG, we first employed differential gene screening. The limma package analysis of RNA-seq data from the TCGA-LGG cohort ($P < 0.05; |\log FC| > 1$) identified 2458 DEGs (Figure 1(A)), including 1449 downregulated and 1009 upregulated genes (Figure 1(B)). To identify key PRs that could affect LGG cell survival, we scored cell lines dependent on 16 primary glioma cell lines and identified 3053 potential genes (Figure 1(C)). Ultimately, we overlapped the 730 reported PRs, the DEGs from the differential analysis and the 3053 potentially lethal genes from the CRISPR-Cas9 screen, and we ultimately identified 24 PRs as specific PRs in LGG (Figure 1(D)), NDUFV2, NDUFB8, SDHC, NAPA, UBR4 NDUFS7, NDUFA9, RPUSD3, PSMA4, MRPL33, STARD7, RPP21, STUB1, ACLY, DDX39B, NDUFS8, CLASRP, RRP9, NXT1, MYC, STON1, CIT, ACTB, and SYT1. In parallel, we employed the ssGSEA algorithm. To further explore the relationship between particular PRs and macrophages, we calculated the number of macrophages in TCGA-LGG tissues. We discovered that most PRs had a negative correlation with the number of macrophages, with CIT showing the strongest negative correlation with DDX39B (Figure 1(E)).

Profiles of specific PRs in LGG

First, we show the locations of specific PRs on 23 chromosomes with altered copy number alterations (CNA (Figure 2(A)), then we report that MYC and NDUFA9 had the highest frequency of CNV amplification while CLASRP and NAPA had the highest frequency of CNV reduction (Figure 2(B)). In addition, we performed a correlation analysis on the 24 PRs and found that most of the PRs' expression was correlated, suggesting a potential regulatory role (Figure 2(C)). Meanwhile, box line plots demonstrated the expression relationships of the 24 PRs in LGG versus normal cortical samples, and interestingly, 8 genes were upregulated, such as *STARD7*, *ACLY*, and *MYC*, while 16 genes were downregulated, such

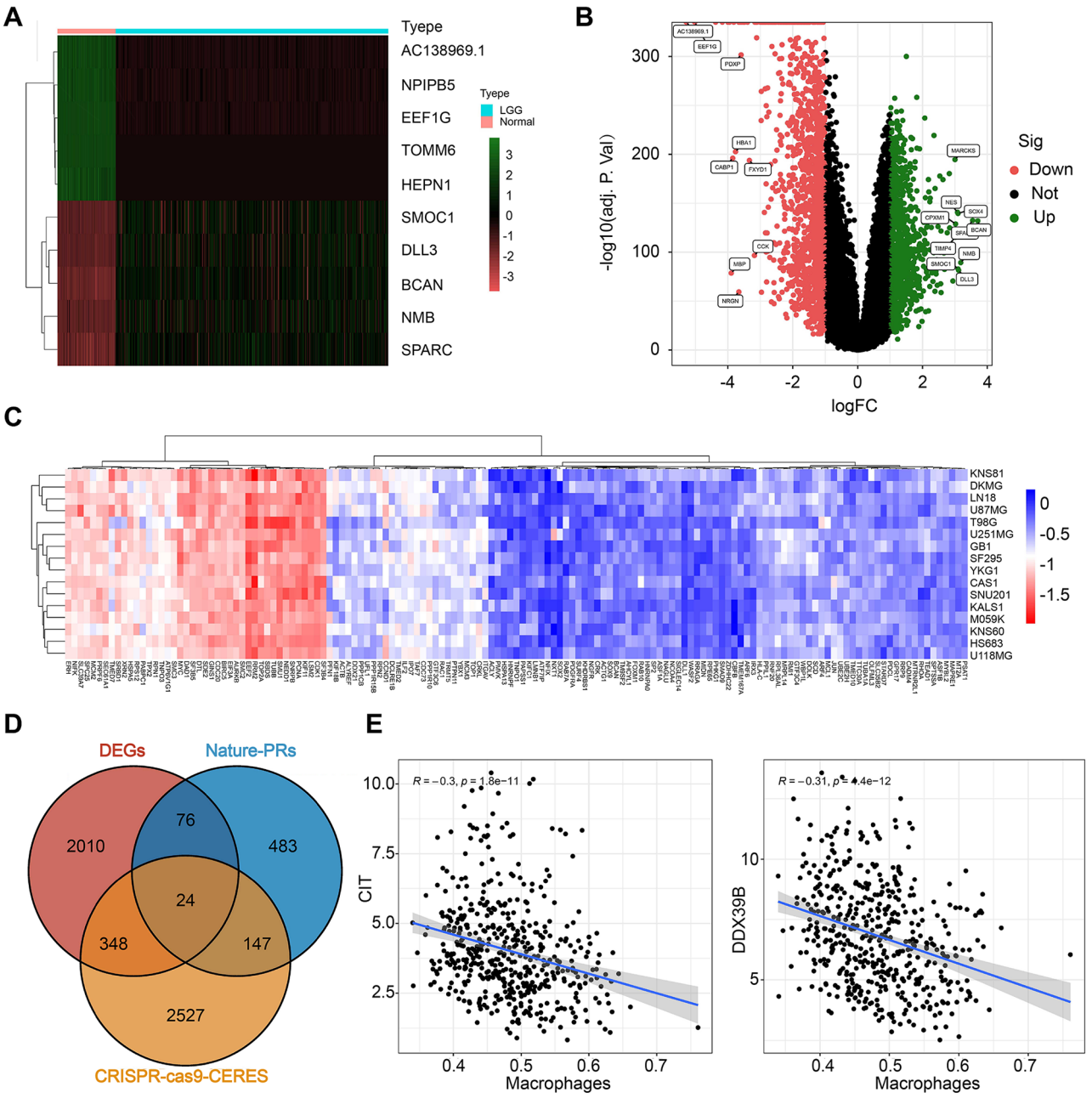

Figure 1. Identification of specific PRs in LGG. (A) and (B) Differential analysis of genes between normal and LGG samples ($P<0.05$;|logFC|>1) identified a total of 2458 DEGs, including 1009 upregulated genes and 1449 downregulated genes, (C) Cell line–dependent scoring of 16 primary glioma cell lines identified 3053 potential genes, (D) Venn diagram showing the identification of 24 PRs as specific PRs in LGG, and (E) Correlation analysis of CIT and DDX39B with macrophage content.

as NDUFP8, SDHC, and NAPA (Figure 2(D)). However, in the mutation frequency study of PRs, only UBR4, CIT, and ACLY had some mutation accumulation in the whole sample (Figure 2(E)).

Molecular typing of PRs mediated by specific PRs

Based on the expression of the 24 specific PRs described above, the NMF consensus clustering method was used to initially classify the molecular subgroups, resulting in three clusters, C1, C2, and C3, in the TCGA-LGG cohort (Supplemental Figure S1(A)). The heat map demonstrates the distribution of PRs expression concerning clinical traits across molecular classifications (Supplemental Figure S1(B)), and it is also worth mentioning that there was a significant difference in survival across molecular subtypes (Supplemental Figure S1(C)). Considering the differences in survival, we speculated that there are different biological processes between the different subtypes and thus used the gene set variation analysis (GSVA) algorithm to enrich gene sets, which showed that glycolysis, gluconeogenesis, and nitrogen metabolism were activated in C1, whereas ribosomes, spliceosomes, and transforming growth factor (TGF) signaling pathways were activated in C2 (Figure 3(A) and (B)). In C3, glutathione metabolism, tyrosine metabolism, and protein metabolism were activated, whereas lysine metabolism,

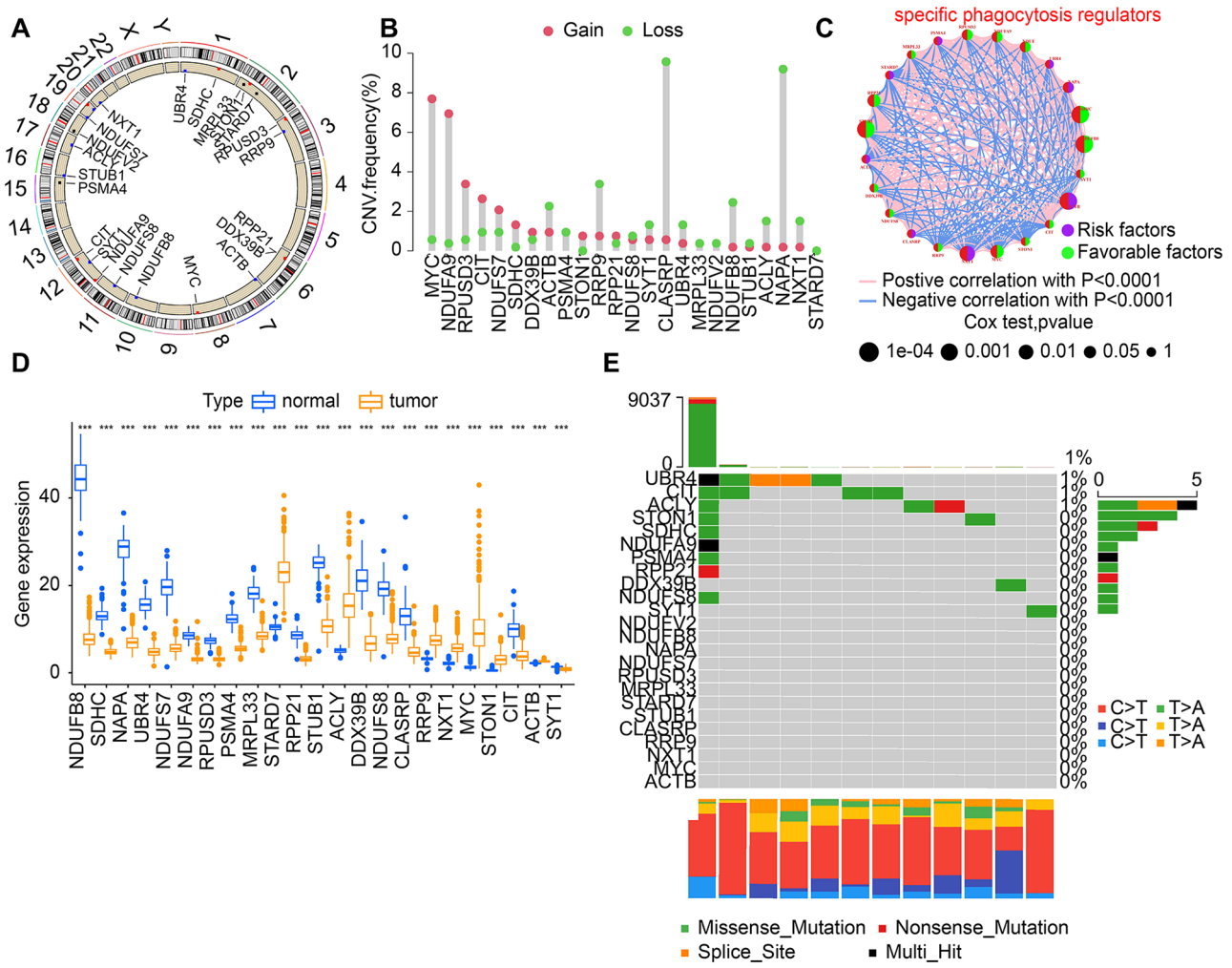

Figure 2. Mutations and transcriptome alterations of PRs in LGG. (A) The location of CNV alterations in PRs on 23 chromosomes is shown in a circular diagram, (B) The CNV frequencies of PRs are given. Red dots represent amplification frequencies, whereas green dots represent deletion frequencies. Numbers indicate the frequency of variation, (C) Network diagram showing the interactions of the 24 PRs in LGG. The *P* value for each gene's impact on survival prognosis is represented by the size of the circles. Green dots indicate favorable factors, whereas red dots indicate risk factors. The correlation value between genes is represented by the line's thickness. Positive and negative gene regulation correlations are depicted by the red and blue lines, respectively, (D) Expression levels of the 24 PRs between tumor and normal samples. Yellow represents tumor, and blue represents normal. Asterisks indicate statistical *P* values ($^{*}P < 0.05$; $^{**}P < 0.01$; $^{***}P < 0.001$), and (E) Mutation frequency of the 24 PRs in LGG.

endocrine disorders, and the phosphatidylinositol signaling system were activated in C2 (Figure 3(C) and (D)). Ribosome, spliceosome, and pyrimidine metabolism were activated in C3, whereas nitrogen metabolism, calcium signaling pathway, and gonadotropin-releasing hormone (GnRH) signaling pathway were activated in C1 (Figure 3(E) and (F)).

Differential genes and genotyping between different molecular typing

Although the identified PRs-cluster is effective in differentiating LGG patients' prognostic outcomes, the fundamental transcriptomic alterations in these subtypes remain unknown. In different molecular subtypes, we investigated the possible mechanisms of action of specific PRs-related genes. DEGs in 433 genes of different molecular subtypes were selected (Supplemental Figure S2(A)). The specific grouping basis for assigning patients to clusters A, B, and C was determined using a clustering algorithm (Supplemental Figure S2(B)). To perform the clustering analysis, we used k-means clustering. These algorithms automatically partitioned glioma patients into distinct groups based on the similarity or dissimilarity of DEGs expression profiles. We classified patients into three subtypes using an unsupervised clustering approach: gene clusters A, B, and C (Supplemental Figure S2(C)). Kaplan–Meier (K-M) survival analysis revealed significant variations between the genetic subtypes, with gene cluster C having the best overall survival (OS) and gene cluster A having the worst OS (Supplemental Figure S2(C)). In addition, we conducted GO enrichment analysis on these DEGs and discovered that enrichment of biological processes was correlated with ribonucleoprotein complex biogenesis, RNA splicing, and spliceosome complexes, while KEGG enrichment analysis revealed the presence of ribosomes, spliceosomes, and mRNA detection pathways. These results further suggest a significant correlation between PRs-related genes and tumorigenesis (Supplemental Figure S2(D) and (E)). In addition, the box line plot results demonstrated that the expression levels of 24 specific PRs differed significantly across various new gene clusters (Supplemental Figure S2(F)).

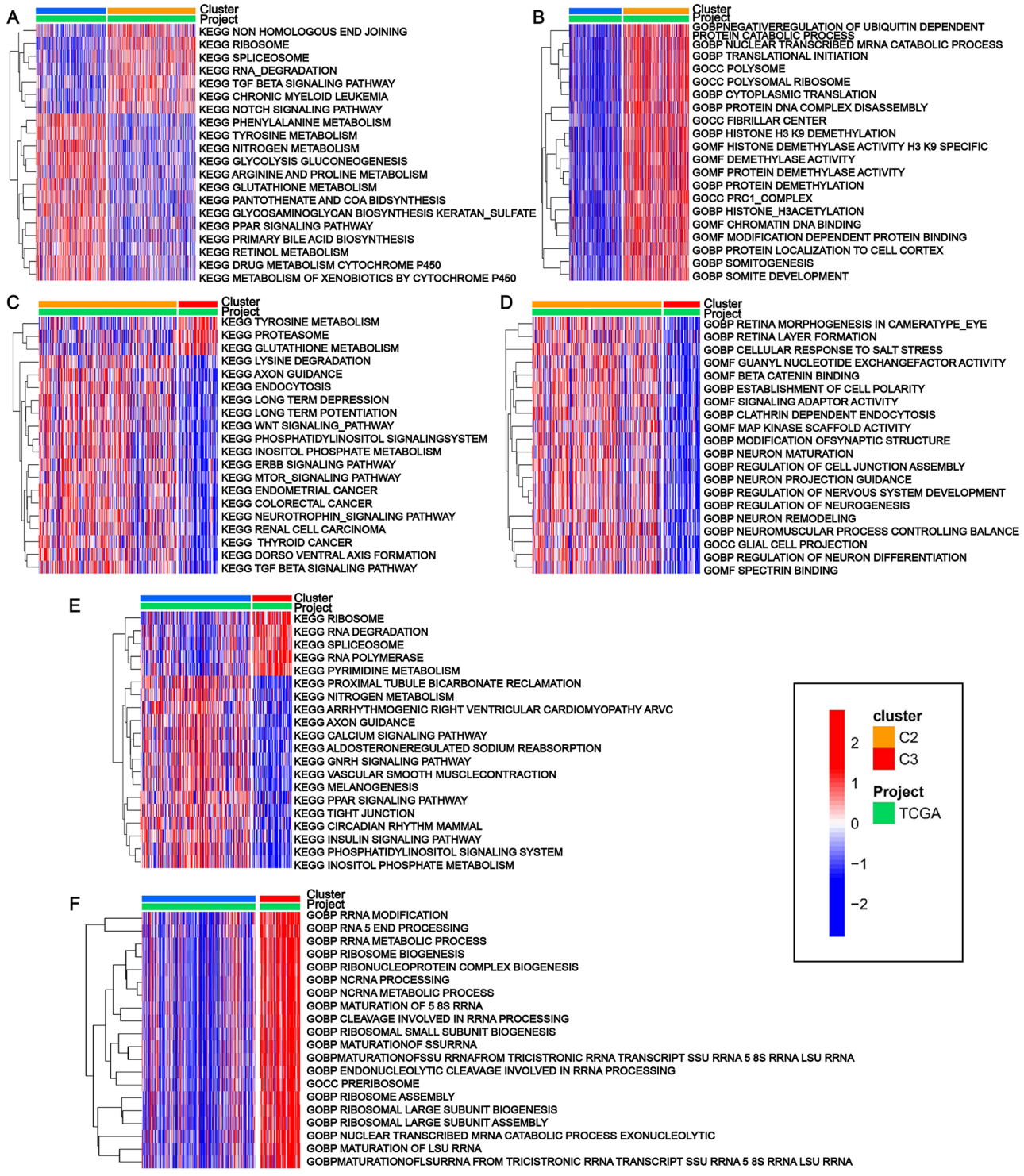

Figure 3. GSVA studied the changes in biological processes between three PRs-clusters. (A) and (B) Comparison of changes in biological processes between C1 and C2, (C) and (D) Comparison of changes in biological processes between C2 and C3, and (E) and (F) Comparison of changes in biological processes between C1 and C3. The heat map shows the biological processes between each cluster.

Construction of PRs-score risk models

To quantify the ADCP status potentially mediated by PRs, we performed Cox-LASSO regression on the TCGA-LGG modeling cohort (Supplemental Figures S3 and 4(A)) and finally screened five PRs for use in constructing the risk equation: PRs-riskscore = (0.4810 × NAPA expression level) + (−0.9068 × NDUFS7 expression level) + (0.2573 × ACLY expression level) + (0.2573 × NXT1 expression level) + (−0.4669 × MYC expression level). Given the importance of tumor mutational burden (TMB) in tumors, we combined the risk and TMB scores and discovered that patients with LGG had the worst prognosis when the risk and TMB scores were both high (Figure 4(B)). Furthermore,

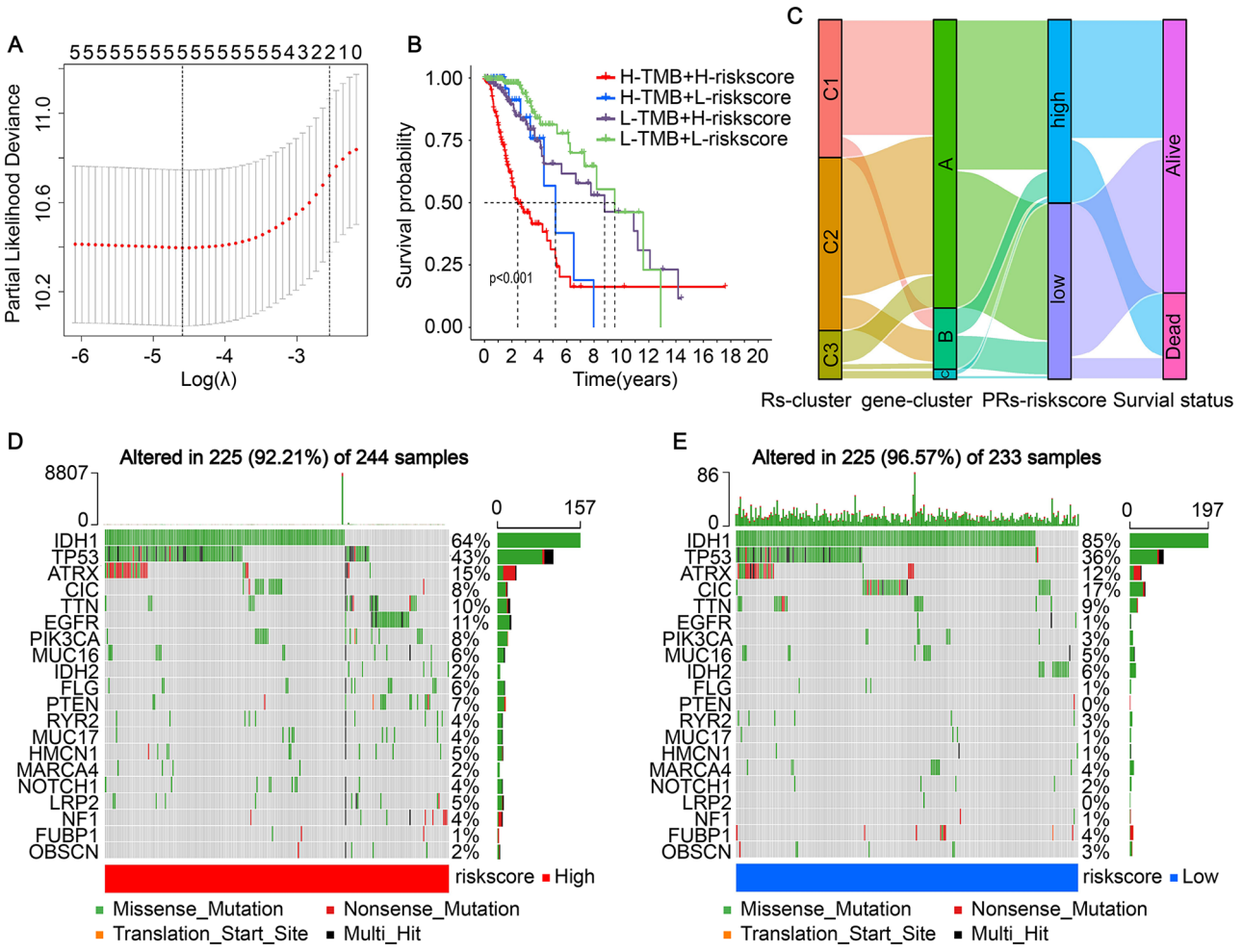

Figure 4. Relationship between the creation of PRs-score and tumor load mutations. (A) The LASSO regression analysis and partial likelihood deviance on the prognostic genes, (B) The difference between the TMB subtype and the PRs-score subtype K-M analysis was statistically significant with a Logrank *P* value < 0.001, (C) SanKey plots with different PRs-clusters, geneClusters, PRs-scores, and clinical outcome groups, (D) and (E) The landscape of tumor somatic mutation in TCGA-LGG displayed by high (D) and low PRs-score (E). Each column represented individual patients. The upper barplot displayed TMB.

we used Mulberry plots to visualize the distribution of risk models, PRs-clusters, and gene clustering, and we found that most C1 subtypes were type A, and most high-risk patients had a death distribution (Figure 4(C)). Furthermore, we predicted mutation frequencies in the low- and high-risk groups and found that TP53, IDH1, and ATRX were significantly mutated genes (Figure 4(D) and (E)).

Validation of the prognostic value of the risk model

The in-progress modeling set and each validation dataset used the same cut-off values to distinguish between high- and low-risk patients. K-M survival analysis in the modeling set showed that low-risk group patients had a better prognosis than the high-risk group patients ($P < 0.001$) (Figure 5(A)). In the internal validation set, patients belonging to the low-risk group had a better prognosis than those belonging to the high-risk group, with the high-risk group having a poor OS ($P < 0.05$) (Figure 5(B)). In addition, multifactorial Cox regression also showed an independent prognostic value for this PRs-riskscore (Figure 5(C)). In the CGGA-LGG-1 cohort, patients belonging to the low-risk group had a better prognosis than those belonging to the high-risk group ($P < 0.005$) (Supplemental Figure S4(A)). In the CGGA-LGG-2 cohort, patients belonging to the low-risk group had a better prognosis than those in the high-risk group ($P < 0.001$) (Supplemental Figure S4(B)). In the GEO-LGG cohort, patients belonging to the low-risk group had a better prognosis than those in the high-risk group ($P < 0.05$) (Supplemental Figure S4(C)). To assess whether the prognostic value of PRs-riskscore was independent of clinicopathological variables, univariate and multifactorial Cox regressions were performed on age, gender, tumor grade, radiotherapy status, chemotherapy status, IDH1 mutation status, combined chromosome 1p/19q deletion status, and PRs-riskscore. The results indicated that PRs-riskscore was an independent prognostic feature of the CGGA cohort ($P < 0.001$) (Supplemental Figure S5(A) and (B)). Similarly, our univariate and multifactorial Cox regressions for age, gender, IDH1 R132 mutation status, KPS score, Type of surgery, and PRs-riskscore in the GEO cohort showed that PRs-riskscore was an independent prognostic feature of the GEO cohort ($P < 0.05$). (Supplemental Figure S5(C) and (D)). In addition, PRs-riskscore showed good discriminating validity across clinical subtypes (Supplemental Figure S6(A) to (L)).

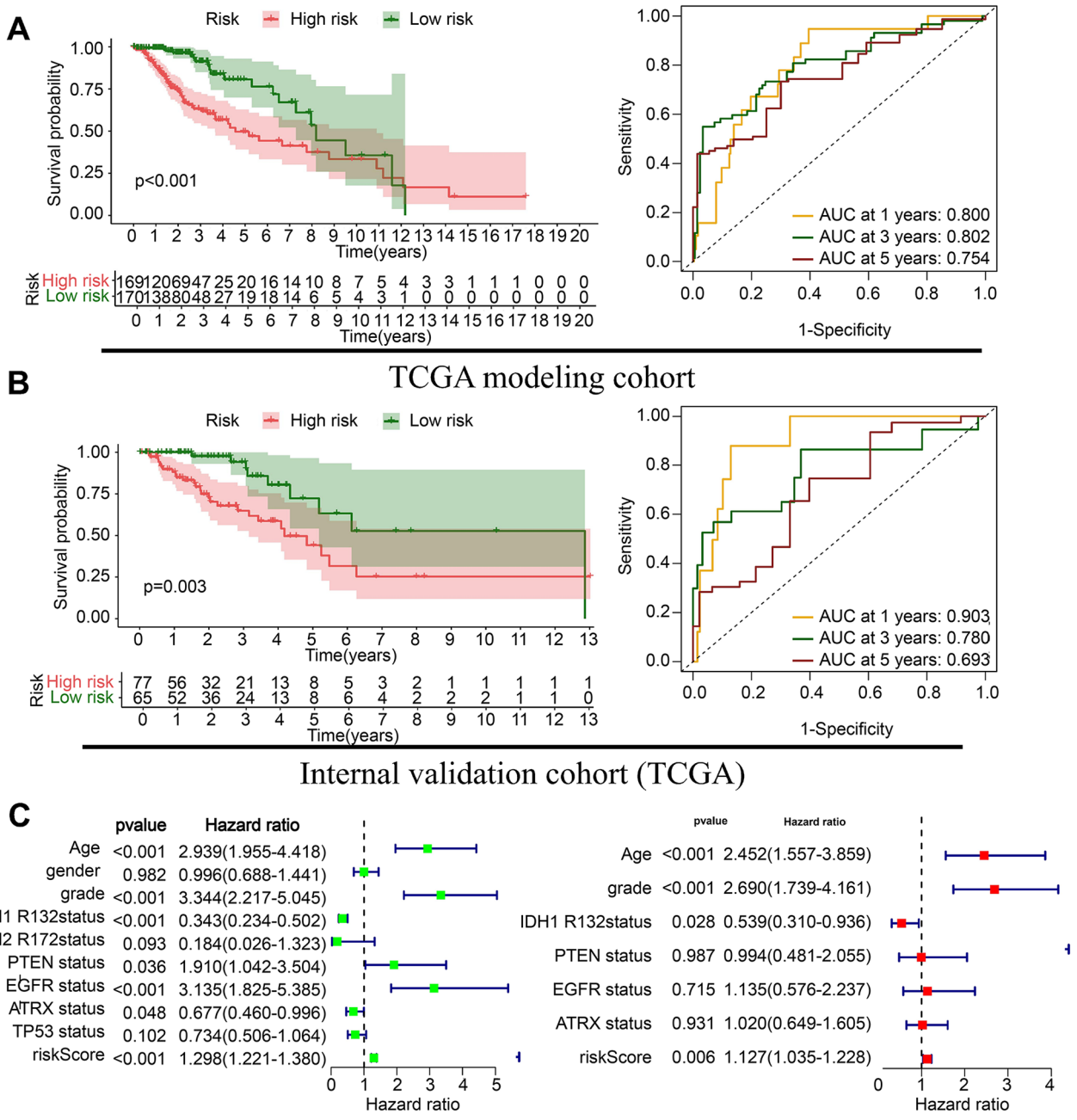

Figure 5. Evaluation of the prognostic significance of risk score in the training cohort. (A) Survival curves and ROC curves for the TCGA modeling cohort, (B) Survival curves and ROC curves for the TCGA internal validation cohort and (C) Forest plot of univariate and multivariate Cox regression analysis of PRs-riskscore and clinicopathological variables in the TCGA cohort.

The pan-cancer landscape for signature genes

The pan-cancer profile and the involvement of these five signature genes in tumor progression have not been thoroughly explored. As a result, it is critical to conduct a thorough investigation of the involvement of these genes in terms of the prognostic significance, expression signature, CNV, SNV, and cancer signaling in various human malignancies. We discovered that most genes are expressed differently between cancerous tissues and normal tissues. In the following study, a total of five signature genes, NAPA, NDUFS7, ACLY, NXT1, and MYC, were analyzed. First, we searched the TCGA database to compare the gene expression of tumor samples with that of normal samples. We discovered that the expression of the genes ACLY, MYC, and NXT1 was generally upregulated in tumor tissues, whereas the expression of NAPA and NDUFS7 was generally downregulated (Figure 6(A)). SNV, CNV, and methylation alterations of these five signature genes, including LGG, were evident. In most cancers, hallmark genes were differentially methylated in comparison to normal tissue; in particular, genes, including MYC, which serves as a representative, were generally hypermethylated, whereas genes, including NDUFS7, NXT1, NAPA, and ACLY, were generally hypomethylated (Figure 6(B)). Substantial CNV deletion was observed in NDUFS7, whereas substantial CNV amplification was

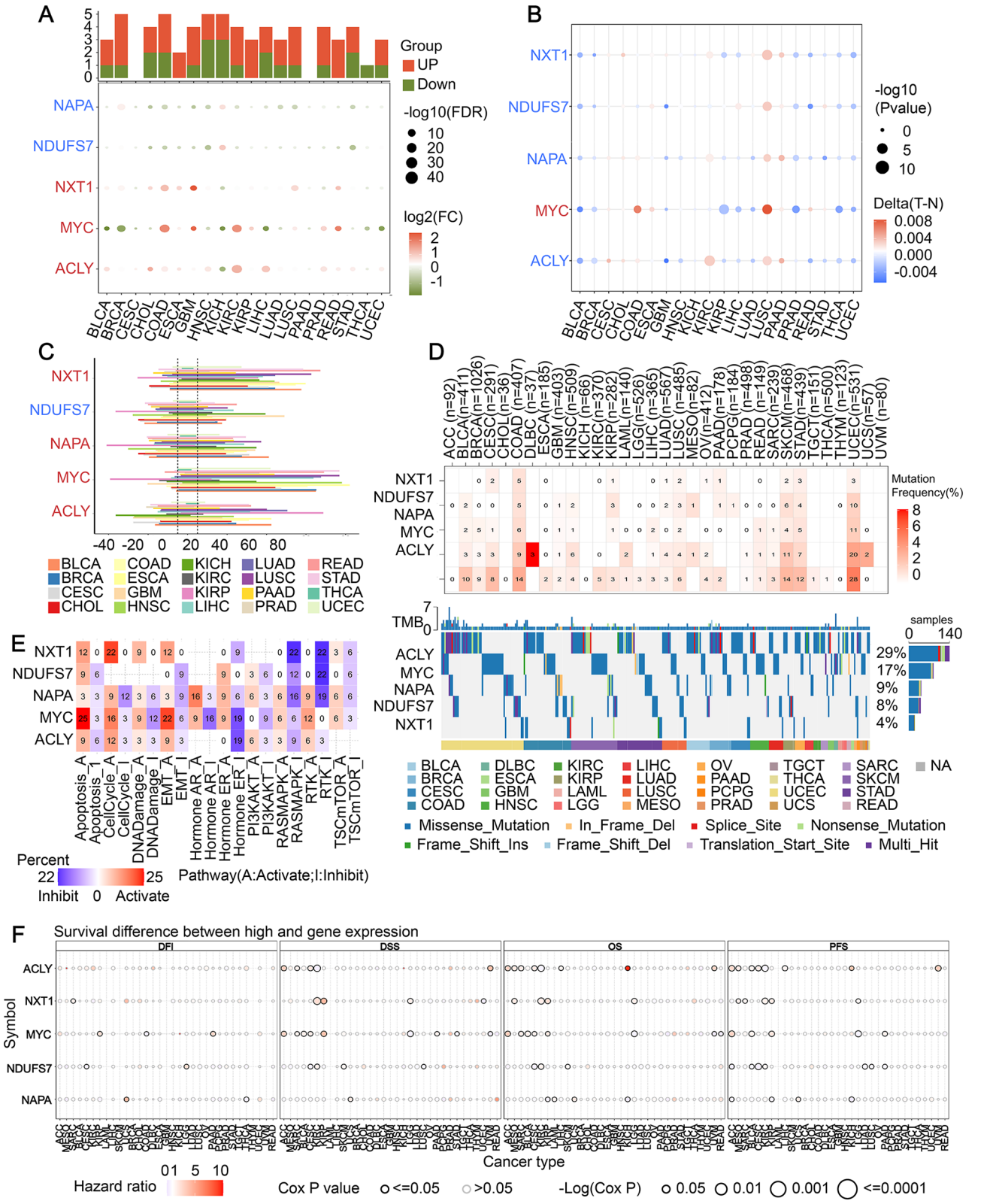

Figure 6. The Pan-cancer landscape for signature genes. (A) The graphs show the log FC and FDR of the signature genes in each cancer. Red and blue indicate genes that are up- and downregulated, (B) Heat map depicting the different methylation of signature genes in malignant tumors; hypermethylated and hypomethylated genes are indicated in red and blue, respectively (Wilcoxon rank-sum test), (C) Bar graph showing the frequency of CNV changes for each signature gene in each cancer type, (D) For a given malignancy, the signature gene mutation frequency represents the number of samples with the mutated gene and the SNV oncoplot, (E) Effect of signature genes on cancer-related pathways (FDR $\leqslant$ 0.05), where numbers in each cell indicate percentages, and (F) The graph shows hazard ratios and Cox *P* values by the color and size of the bubbles. The rows are genomic symbols and the columns are selected cancer types. The color of the bubbles ranges from blue to red representing low to high hazard ratios and the size of the bubbles is positively correlated with the significance of the Cox *P* value. The black outline border indicates a Cox *P* value $\leqslant$ 0.05.

observed in most tumor types in NXT1, NAPA, MYC, and ACLY (Figure 6(C)); substantial SNV alterations were observed in NDUFS7, NXT1, NAPA, MYC, and ACLY most tumor types (Figure 6(D)). The potential effects of these five signature genes on several bioactive pathways are then discussed in depth. Briefly, it can be observed that PANoptosis genes may generally activate pathway activity, such as apoptosis, and inhibit RTK pathway activity. Furthermore, Figure 6(E) shows that these five signature genes may be linked to numerous biologically relevant pathways. Following this, we created a survival profile of these genes based on the relationship between TCGA-recorded gene expression levels and patient survival (Figure 6(F)).

Immune infiltration analysis of risk models and implications for immunotherapy

To elucidate the pattern of immune cell infiltration, we performed ssGSEA on 28 tumor-infiltrating lymphocytes (TILs) extracted from the Cancer Immunome Atlas. PRs-riskscore was found to be positively linked to effector memory CD4 cells, memory B cells, central memory CD4 and CD8T cells, and memory B cells (Supplemental Figure S7(A)). This implies that people with high PRs-risk scores have better long-term T and B cell–mediated adaptive antitumor immunity. In addition, the high-risk score group showed evidence of macrophage infiltration, but its function is unknown. We found that the high-risk score group had a significant Treg cell infiltration, suggesting an immunosuppressive effect in high-riskscore tumors. We conducted an ssGSEA on the relationship between riskscore and the cancer-immune cycle to test this hypothesis. Riskscore linked negatively to Th1 helper cells and positively to Th2 and Treg cell recruitment, as was hypothesized (Supplemental Figure S7(B)). In LGG tumors with high riskscores, Th1/Th2 helper cell imbalance and Treg cell recruitment showed reduced antitumor immunity. Since the high-risk score group was immunosuppressed, we compared immune checkpoint marker levels across the two groups to see if immune checkpoints contributed to their immunosuppression. In the high-risk score group, we observed a substantial elevation of the expression levels of VSIR, NPR1, and TNFSF9 genes (Supplemental Figure S8(A)). The heat map (Supplemental Figure S8(B)) showed that this group had a lot of PD1 receptors. This suggests that treatment for immune checkpoints could target these markers. In addition, we conducted CMap analysis to find prospective compounds that target genes that are expressed differentially in MS groups and their underlying processes. Phenothiazine and brinzolamide are two carbonic anhydrase inhibitors that we discovered (Supplemental Figure S8(C)). These findings offer LGG patients having high riskscores with promising therapy options.

Construction of an optimal radiomic profile

We developed 9504 models using the AUC values of the classifier test group as the best selection criteria by integrating several material methods. We were able to identify the best imaging genomics models for prediction using Z-score normalization (Figure 7(A)), the recursive feature elimination (RFE) method (Figure 7(B)), and the PCA method (Figure 7(C)) for dimensionality reduction and preprocessing, and finally, nine imaging optimal features (Figure 7(E)) created using the AB method (Figure 7(D)). For the internal validation dataset, we discovered that these nine features resulted in the model with the highest AUC value. AUC degrees for the model on the training and test datasets were 0.868 and 0.686, respectively, at this point (Figure 7(F)).

Discussion

LGG is a prevalent malignant tumor affecting the CNS. Reliable treatment targets may have the potential to improve the survival of patients with LGG. Tolerance, initiation, and M1 or M2 activation are macrophages' classical adaptive responses.[42,43] Macrophages generate crucial immunosuppressive mediators, such as prostaglandins, IL-10, and arginase (enzymes involved in amino acid metabolism) and T- and NK-cell immune checkpoint inhibitory triggers (e.g. PD-L1, VISTA).[44] Macrophage phagocytosis is a critical component of immune system regulation, and severe macrophage disorders contribute to tumor growth and development. Phagocytosis is involved in the expulsion of cell debris following injury, the clearing of apoptotic cells, cell regeneration, tumor surveillance, and other disease processes.[45] In addition, autoimmune and developmental abnormalities can occur when phagocytosis is out of balance.[46] Furthermore, phagocytes use different surface receptors and signaling cascades to phagocytose different types of particles.[47] Notably, the removal of cancer cells occurs following macrophage phagocytosis, which is triggered by monoclonal antibody treatment that targets tumor antigens.[35] It is now crucial to identify the regulators linked to antibody-dependent cytophagocytosis to treat tumors. The macrophage phagocytosis factors are critical components of the complex gene network that regulates macrophage activation, polarization, and adaptability.[48] Combining macrophage phagocytosis factors with novel immunotherapy regimens for cancer treatment is a very promising technique.[49]

Therefore, it is crucial to find macrophage phagocytosis factor-related biomarkers to identify LGG patients for early intervention or treatment. We know that various inhibitory and stimulatory signals influence cancer cell phagocytosis and immune recognition, which needs to be addressed to optimize the antitumor response. Fortunately, modern genetic screening tools may be used in the oncological immune milieu to uncover PRs under physiological settings and non-tumorigenic pathology. For example, the recently popular CRISPR-Cas9 gene-editing technology has given gene editing a major boost as the first tool in biomedical history to efficiently, precisely, and programmatically modify the genome. CRISPR has emerged as a unique tool for oncology drug target discovery and can be used to mutate, suppress, or activate any targeted human gene. CRISPR-Cas9 screening systems based on sgRNA libraries can help us understand gene function and gene expression's effect on cells. The advancement of CRISPR-Cas9-based gene-editing methods represents a significant breakthrough in biology.[50,51] CRISPR-Cas9 libraries are an excellent resource for identifying critical genes involved in cancer cell survival and therapy.[52]

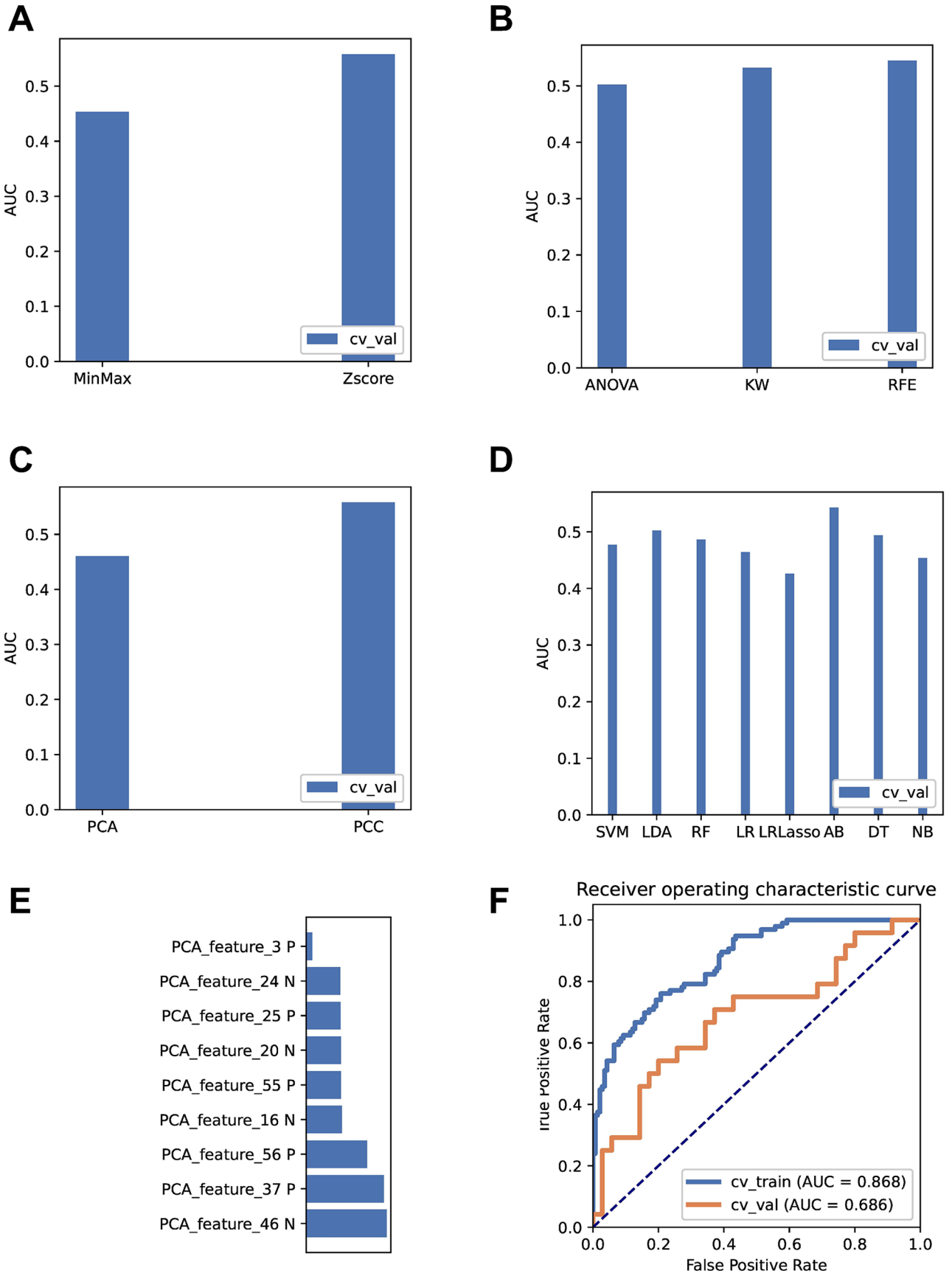

Figure 7. Establishment of radiomics model. (A) The effect on the AUC values of the radiomics model when different methods of normalizing the imaging data are used, (B) Impact of feature selection methods on classifier AUC values during radiogenomics model building, (C) Effect of the choice of feature reduction method on the AUC value of the model, (D) Comparing the effectiveness of various machine learning modeling approaches on the classifier performance in the test set, including LR, LDA, RF, LR-lasso, NB, DT, SVM, and AB, revealing that AB performed the best, (E) The final radiogenomics model's weighting coefficients of the retrieved features and (F) Results of the best classifier model's AUC values in the training and test groups.

In this study, we combined previously reported CRISPR-Cas9 screens for genes that differ in expression between normal and LGG tissues in TCG, regulators of cancer cell phagocytosis, and CRISPR-Cas9 screens for $|\text{CERES}| > 0.5$ that are crucial for the survival and proliferation of LGG cell lines. Based on the above 24 specific PRs, we provided a comprehensive analysis of expression differences, CNV, SNV, and prognostic features. However, the NMF consensus clustering approach was used to first categorize molecular subgroups and then identify three PRs in the TCGA-LGG cohort clusters, namely, C1, C2, and C3, and the GSVA algorithm was used to comprehend variations in TME across the three PRs-clusters. Because TME is critical for immune evasion, local treatment resistance, and distant tumor metastasis, its composition influences cancer immunophenotypes and patient prognosis.[53] Even though the detected PRs-cluster can successfully predict the prognosis of LGG patients, the underlying transcriptome alterations in these subtypes are unknown. To this end, we were able to establish three genetic subtypes, genecluster A, B, and C, using DEGs across the three PRs-clusters. We show that macrophage phagocytosis factor expression is strongly related to prognosis and TME in LGG. Most importantly, we developed and validated prognostic risk profiles for five signature genes (NAPA, NDUFS7, ACLY, NXT1, and MYC), classifying LGG patients into high- and low-risk groups. NSF attachment protein alpha (NAPA) is a ubiquitous and essential component of the membrane fusion machinery. In the embryo, NAPA deletion is fatal. However, minor changes in NAPA expression levels are linked to a variety of pathological conditions, including several neurological diseases, type 2 diabetes, and aggressive neuroendocrine tumors.[54,55] NDUFS7 (NADH: Ubiquinone Oxidoreductase Core Subunit S7) is an ATP citrate lyase (ACLY). It is a key enzyme in cellular metabolism and is a major source of acetyl coenzyme A, an important precursor for the biosynthesis of fatty acids, cholesterol, and isoprene, and is also involved in protein acetylation.[56] Its expression has been shown to be linked to hyperlipidemia and cardiovascular disease. Other studies have highlighted its importance for cancer progression[57] and lipid-related diseases.[58] Several other experimental studies have that elevated ACLY expression level that is found in many different tumors and that upregulation of ACLY expression regulates the proliferation, growth, and invasiveness of cancer cells, including gastric adenocarcinoma,[59] hepatocellular carcinoma,[60] breast cancer,[61] and colon cancer.[62] Nuclear transport factor 2 like export factor 1 (NXT1) shuttles between the nucleus and cytoplasm of postnatal animal cells and contributes to the nuclear export of a variety of RNAs, but the genetic profile of these molecules has not been thoroughly characterized.[63] MYC is critical in circulating progenitor cells born from the proliferative zone during embryonic development and in all proliferating cells after birth since the discovery of the oncogene carried by the avian acute leukemia virus MC29 in myeloblastomatosis[64] and its clone.[65] In some cell types and environments, MYC deletion results in cell cycle exit or cell death, whereas MYC amplification or overexpression enhances cell proliferation and is present in many malignancies.

Furthermore, PRs-riskscore is also an independent LGG prognostic biomarker with high predictive value for OS and immunotherapy, among others. Finally, to better serve the clinical management, we attempted to distinguish high-risk and low-risk LGG patients early based on their preoperative head MRI images using multiple machine learning classifiers, including plain Bayes, logistic regression, random forest, SVM, AdaBoost, LR-Lasso, and LDA for radiogenomics. When the classifier model had nine features, it had AUC degrees of 0.868 and 0.686 for the training and test datasets, indicating high diagnostic efficacy. It is unclear how these phagocytic regulators influence professional phagocytes' tumor cell clearance at different stages of tumorigenesis and in different cancers. More investigation is required from a clinical perspective to ascertain how phagocytic checkpoint blockers/stimulators might be added to the present cancer immunotherapy paradigm. First, to maximize antitumor responses, phagocytic checkpoints should be targeted in addition to T cell immune checkpoint inhibitors now in use. Tumors with low PD-L1 levels, for example, are less sensitive to PD-1/PD-L1 axis blockade and may be more sensitive to CD47-SIRPα interference. Similarly, adaptive immunotherapy is based on the generation of specific T cell clones that recognize tumor-associated neoantigens, which is correlated with the degree of genomic alteration in tumor cells, and phagocytic checkpoint blockade appears to be effective in cancers with low mutational burden (e.g. AML). As a result, a comprehensive PR analysis is required for immunotherapy and prognostic prediction in patients with LGG.

This study, however, only collected data from the public databases TCGA and CGGA to develop the model and was not conditioned to collect our data to verify the PRs signature, which is a drawback of our work. We also limited our attention to PRs in LGG cell lines, and further experimental verification is required. To further validate our immune assessment results, we plan to conduct IHC experiments to investigate the expression of specific immune-related markers, such as CD3, CD8, PD-L1, and others. These experiments will allow us to visualize and quantify the presence and localization of immune cells within the tumor tissues.

Conclusions

We developed an accurate and robust PR signature for predicting the prognosis of LGG patients. We discovered an interaction between the tumor microenvironment and LGG patient-specific PRs as a result of this. Different risk groups, in particular, may represent different ADCP states in LGG patients. Most importantly, our proposed radiogenomic model is a non-invasive predictive approach combining radiomic and genomic features and has shown effective and sufficient performance in predicting treatment response and survival outcomes in LGG patients. Further interdisciplinary studies combining medicine and electronics are yet to be explored.

AUTHORS' CONTRIBUTIONS

AM and AA involved in conceptualization, methodology, validation, investigation, supervision, visualization, writing – original draft, and writing – reviewing. BT, YD, XL, SY, YW, LJ,

and HS participated in the coordination of data acquisition and data analysis and reviewed the article. All authors read and approved the final version of the article.

DECLARATION OF CONFLICTING INTERESTS

The author(s) declared no potential conflicts of interest with respect to the research, authorship, and/or publication of this article.

FUNDING

The author(s) disclosed receipt of the following financial support for the research, authorship, and/or publication of this article: This work was supported by the Xinjiang Uygur Autonomous Region Science and technology Project (Grant No. 2020D01C230).

ORCID ID

Hua Shao https://orcid.org/0009-0006-9185-917X

SUPPLEMENTAL MATERIAL

Supplemental material for this article is available online.

REFERENCES

1. Gittleman H, Sloan AE, Barnholtz-Sloan JS. An independently validated survival nomogram for lower-grade glioma. *Neuro Oncol* 2020;**22**:665–74
2. Liu Z, Ji H, Fu W, Ma S, Zhao H, Wang F, Dong J, Yan X, Zhang J, Wang N, Wu J, Hu S. IGFBPs were associated with stemness, inflammation, extracellular matrix remodeling and poor prognosis of low-grade glioma. *Front Endocrinol* 2022;**13**:943300
3. Sun Y, Sedgwick AJ, Palarasah Y, Mangiola S, Barrow AD. A transcriptional signature of PDGF-DD activated natural killer cells predicts more favorable prognosis in low-grade glioma. *Front Immunol* 2021;**12**:668391
4. Gargini R, Segura-Collar B, Herránz B, García-Escudero V, Romero-Bravo A, Núñez FJ, García-Pérez D, Gutiérrez-Guamán J, Ayuso-Sacido A, Seoane J, Pérez-Núñez A, Sepúlveda-Sánchez JM, Hernández-Laín A, Castro MG, García-Escudero R, Ávila J, Sánchez-Gómez P. The IDH-TAU-EGFR triad defines the neovascular landscape of diffuse gliomas. *Sci Transl Med* 2020;**12**:eaax1501
5. Van den Bent MJ. Practice changing mature results of RTOG study 9802: another positive PCV trial makes adjuvant chemotherapy part of standard of care in low-grade glioma. *Neuro Oncol* 2014;**16**:1570–4
6. Yoshihara K, Shahmoradgoli M, Martínez E, Vegesna R, Kim H, Torres-Garcia W, Treviño V, Shen H, Laird PW, Levine DA, Carter SL, Getz G, Stemke-Hale K, Mills GB, Verhaak RGW. Inferring tumour purity and stromal and immune cell admixture from expression data. *Nat Commun* 2013;**4**:2612
7. Ge PL, Li SF, Wang WW, Li CB, Fu YB, Feng ZK, Li L, Zhang G, Gao ZQ, Dang XW, Wu Y. Prognostic values of immune scores and immune microenvironment-related genes for hepatocellular carcinoma. *Aging* 2020;**12**:5479–99
8. Ngambenjawong C, Gustafson HH, Pun SH. Progress in tumor-associated macrophage (TAM)-targeted therapeutics. *Adv Drug Deliv Rev* 2017;**114**:206–21
9. Yan S, Wan G. Tumor-associated macrophages in immunotherapy. *FEBS J* 2021;**288**:6174–86
10. DeNardo DG, Ruffell B. Macrophages as regulators of tumour immunity and immunotherapy. *Nat Rev Immunol* 2019;**19**:369–82
11. Cassetta L, Pollard JW. Targeting macrophages: therapeutic approaches in cancer. *Nat Rev Drug Discov* 2018;**17**:887–904
12. Biswas SK, Mantovani A. Macrophage plasticity and interaction with lymphocyte subsets: cancer as a paradigm. *Nat Immunol* 2010;**11**:889–96
13. Chen D, Xie J, Fiskesund R, Dong W, Liang X, Lv J, Jin X, Liu J, Mo S, Zhang T, Cheng F, Zhou Y, Zhang H, Tang K, Ma J, Liu Y, Huang B. Chloroquine modulates antitumor immune response by resetting tumor-associated macrophages toward M1 phenotype. *Nat Commun* 2018;**9**:873
14. Pathria P, Louis TL, Varner JA. Targeting tumor-associated macrophages in cancer. *Trends Immunol* 2019;**40**:310–27
15. Miao L, Qi J, Zhao Q, Wu QN, Wei DL, Wei XL, Liu J, Chen J, Zeng ZL, Ju HQ, Luo HY, Xu RH. Targeting the STING pathway in tumor-associated macrophages regulates innate immune sensing of gastric cancer cells. *Theranostics* 2020;**10**:498–515
16. Logtenberg MEW, Scheeren FA, Schumacher TN. The CD47-SIRPα immune checkpoint. *Immunity* 2020;**52**:742–52
17. Gordon SR, Maute RL, Dulken BW, Hutter G, George BM, McCracken MN, Gupta R, Tsai JM, Sinha R, Corey D, Ring AM, Connolly AJ, Weissman IL. PD-1 expression by tumour-associated macrophages inhibits phagocytosis and tumour immunity. *Nature* 2017;**545**:495–9
18. Mantovani A, Marchesi F, Malesci A, Laghi L, Allavena P. Tumour-associated macrophages as treatment targets in oncology. *Nat Rev Clin Oncol* 2017;**14**:399–416
19. Kocak B, Durmaz ES, Ates E, Sel I, Turgut Gunes S, Kaya OK, Zeynalova A, Kilickesmez O. Radiogenomics of lower-grade gliomas: machine learning-based MRI texture analysis for predicting 1p/19q codeletion status. *Eur Radiol* 2020;**30**:877–86
20. Beer L, Sahin H, Bateman NW, Blazic I, Vargas HA, Veeraraghavan H, Kirby J, Fevrier-Sullivan B, Freymann JB, Jaffe CC, Brenton J, Miccó M, Nougaret S, Darcy KM, Maxwell GL, Conrads TP, Huang E, Sala E. Integration of proteomics with CT-based qualitative and radiomic features in high-grade serous ovarian cancer patients: an exploratory analysis. *Eur Radiol* 2020;**30**:4306–16
21. Kim M, Jung SY, Park JE, Jo Y, Park SY, Nam SJ, Kim JH, Kim HS. Diffusion- and perfusion-weighted MRI radiomics model may predict isocitrate dehydrogenase (IDH) mutation and tumor aggressiveness in diffuse lower grade glioma. *Eur Radiol* 2020;**30**:2142–51
22. Zhang J, Zhao X, Zhao Y, Zhang J, Zhang Z, Wang J, Wang Y, Dai M, Han J. Value of pre-therapy ^{18}F-FDG PET/CT radiomics in predicting EGFR mutation status in patients with non-small cell lung cancer. *Eur J Nucl Med Mol Imaging* 2020;**47**:1137–46
23. Wei J, Yang G, Hao X, Gu D, Tan Y, Wang X, Dong D, Zhang S, Wang L, Zhang H, Tian J. A multi-sequence and habitat-based MRI radiomics signature for preoperative prediction of MGMT promoter methylation in astrocytomas with prognostic implication. *Eur Radiol* 2019;**29**:877–88
24. Yang L, Gu D, Wei J, Yang C, Rao S, Wang W, Chen C, Ding Y, Tian J, Zeng M. A radiomics nomogram for preoperative prediction of microvascular invasion in hepatocellular carcinoma. *Liver Cancer* 2019;**8**:373–86
25. Hu LS, Ning S, Eschbacher JM, Baxter LC, Gaw N, Ranjbar S, Plasencia J, Dueck AC, Peng S, Smith KA, Nakaji P, Karis JP, Quarles CC, Wu T, Loftus JC, Jenkins RB, Sicotte H, Kollmeyer TM, O'Neill BP, Elmquist W, Hoxworth JM, Frakes D, Sarkaria J, Swanson KR, Tran NL, Li J, Mitchell JR. Radiogenomics to characterize regional genetic heterogeneity in glioblastoma. *Neuro Oncol* 2017;**19**:128–37
26. Pennisi E. The CRISPR craze. *Science* 2013;**341**:833–6
27. Chen M, Mao A, Xu M, Weng Q, Mao J, Ji J. CRISPR-Cas9 for cancer therapy: opportunities and challenges. *Cancer Lett* 2019;**447**:48–55
28. Cong L, Ran FA, Cox D, Lin S, Barretto R, Habib N, Hsu PD, Wu X, Jiang W, Marraffini LA, Zhang F. Multiplex genome engineering using CRISPR/Cas systems. *Science* 2013;**339**:819–23
29. Mali P, Yang L, Esvelt KM, Aach J, Guell M, DiCarlo JE, Norville JE, Church GM. RNA-guided human genome engineering via Cas9. *Science* 2013;**339**:823–6
30. Zhan T, Rindtorff N, Betge J, Ebert MP, Boutros M. CRISPR/Cas9 for cancer research and therapy. *Semin Cancer Biol* 2019;**55**:106–19
31. Zheng N, Li L, Wang X. Molecular mechanisms, off-target activities, and clinical potentials of genome editing systems. *Clin Transl Med* 2020;**10**:412–26
32. Qi LS, Larson MH, Gilbert LA, Doudna JA, Weissman JS, Arkin AP, Lim WA. Repurposing CRISPR as an RNA-guided platform for sequence-specific control of gene expression. *Cell* 2013;**152**:1173–83

33. Perez-Pinera P, Kocak DD, Vockley CM, Adler AF, Kabadi AM, Polstein LR, Thakore PI, Glass KA, Ousterout DG, Leong KW, Guilak F, Crawford GE, Reddy TE, Gersbach CA. RNA-guided gene activation by CRISPR-Cas9-based transcription factors. *Nat Methods* 2013;**10**:973–6
34. Gilbert LA, Larson MH, Morsut L, Liu Z, Brar GA, Torres SE, Stern-Ginossar N, Brandman O, Whitehead EH, Doudna JA, Lim WA, Weissman JS, Qi LS. CRISPR-mediated modular RNA-guided regulation of transcription in eukaryotes. *Cell* 2013;**154**:442–51
35. Kamber RA, Nishiga Y, Morton B, Banuelos AM, Barkal AA, Vences-Catalán F, Gu M, Fernandez D, Seoane JA, Yao D, Liu K, Lin S, Spees K, Curtis C, Jerby-Arnon L, Weissman IL, Sage J, Bassik MC. Inter-cellular CRISPR screens reveal regulators of cancer cell phagocytosis. *Nature* 2021;**597**:549–54
36. Meyers RM, Bryan JG, McFarland JM, Weir BA, Sizemore AE, Xu H, Dharia NV, Montgomery PG, Cowley GS, Pantel S, Goodale A, Lee Y, Ali LD, Jiang G, Lubonja R, Harrington WF, Strickland M, Wu T, Hawes DC, Zhivich VA, Wyatt MR, Kalani Z, Chang JJ, Okamoto M, Stegmaier K, Golub TR, Boehm JS, Vazquez F, Root DE, Hahn WC, Tsherniak A. Computational correction of copy number effect improves specificity of CRISPR-Cas9 essentiality screens in cancer cells. *Nat Genet* 2017;**49**:1779–84
37. Ye Y, Xiang Y, Ozguc FM, Kim Y, Liu CJ, Park PK, Hu Q, Diao L, Lou Y, Lin C, Guo AY, Zhou B, Wang L, Chen Z, Takahashi JS, Mills GB, Yoo SH, Han L. The genomic landscape and pharmacogenomic interactions of clock genes in cancer chronotherapy. *Cell Syst* 2018;**6**:314.e2–28.e2
38. Rorden C, Brett M. Stereotaxic display of brain lesions. *Behav Neurol* 2000;**12**:191–200
39. Zhang L, Giuste F, Vizcarra JC, Li X, Gutman D. Radiomics features predict CIC mutation status in lower grade glioma. *Front Oncol* 2020;**10**:937
40. Van Griethuysen JJM, Fedorov A, Parmar C, Hosny A, Aucoin N, Narayan V, Beets-Tan RGH, Fillion-Robin JC, Pieper S, Aerts H. Computational radiomics system to decode the radiographic phenotype. *Cancer Res* 2017;**77**:e104–7
41. Song Y, Zhang J, Zhang YD, Hou Y, Yan X, Wang Y, Zhou M, Yao YF, Yang G. FeAture Explorer (FAE): a tool for developing and comparing radiomics models. *PLoS One* 2020;**15**:e0237587
42. Locati M, Curtale G, Mantovani A. Diversity, mechanisms, and significance of macrophage plasticity. *Annu Rev Pathol* 2020;**15**:123–47
43. Raggi F, Pelassa S, Pierobon D, Penco F, Gattorno M, Novelli F, Eva A, Varesio L, Giovarelli M, Bosco MC. Regulation of human macrophage M1-M2 polarization balance by hypoxia and the triggering receptor expressed on myeloid cells-1. *Front Immunol* 2017;**8**:1097
44. Groth C, Hu X, Weber R, Fleming V, Altevogt P, Utikal J, Umansky V. Immunosuppression mediated by myeloid-derived suppressor cells (MDSCs) during tumour progression. *Br J Cancer* 2019;**120**:16–25
45. Lim JJ, Grinstein S, Roth Z. Diversity and versatility of phagocytosis: roles in innate immunity, tissue remodeling, and homeostasis. *Front Cell Infect Microbiol* 2017;**7**:191
46. Gordon S. Phagocytosis: an immunobiologic process. *Immunity* 2016;**44**:463–75
47. Freeman SA, Grinstein S. Phagocytosis: receptors, signal integration, and the cytoskeleton. *Immunol Rev* 2014;**262**:193–215
48. Orecchioni M, Ghosheh Y, Pramod AB, Ley K. Macrophage polarization: different gene signatures in M1(LPS+) vs. classically and M2(LPS-) vs. alternatively activated macrophages. *Front Immunol* 2019;**10**:1084
49. Kumari N, Choi SH. Tumor-associated macrophages in cancer: recent advancements in cancer nanoimmunotherapies. *J Exp Clin Cancer Res* 2022;**41**:68
50. Morgens DW, Deans RM, Li A, Bassik MC. Systematic comparison of CRISPR/Cas9 and RNAi screens for essential genes. *Nat Biotechnol* 2016;**34**:634–6
51. Onishi I, Yamamoto K, Kinowaki Y, Kitagawa M, Kurata M. To discover the efficient and novel drug targets in human cancers using CRISPR/Cas screening and databases. *Int J Mol Sci* 2021;**22**:12322
52. Sanjana NE, Shalem O, Zhang F. Improved vectors and genome-wide libraries for CRISPR screening. *Nat Methods* 2014;**11**:783–4
53. Chen F, Zhuang X, Lin L, Yu P, Wang Y, Shi Y, Hu G, Sun Y. New horizons in tumor microenvironment biology: challenges and opportunities. *BMC Med* 2015;**13**:45
54. Wang J, Luo J, Wen Z, Wang X, Shuai L, Zhong G, Wang C, Sun Z, Chen W, Ge J, Liu R, Wang X, Bu Z. Alpha-soluble NSF attachment protein prevents the cleavage of the SARS-CoV-2 spike protein by functioning as an interferon-upregulated furin inhibitor. *mBio* 2022;**13**:e0244321
55. Andreeva AV, Kutuzov MA, Voyno-Yasenetskaya TA. A ubiquitous membrane fusion protein alpha SNAP: a potential therapeutic target for cancer, diabetes and neurological disorders? *Expert Opin Ther Targets* 2006;**10**:723–33
56. Fan F, Williams HJ, Boyer JG, Graham TL, Zhao H, Lehr R, Qi H, Schwartz B, Raushel FM, Meek TD. On the catalytic mechanism of human ATP citrate lyase. *Biochemistry* 2012;**51**:5198–211
57. Icard P, Wu Z, Fournel L, Coquerel A, Lincet H, Alifano M. ATP citrate lyase: a central metabolic enzyme in cancer. *Cancer Lett* 2020;**471**:125–34
58. Burke AC, Huff MW. ATP-citrate lyase: genetics, molecular biology and therapeutic target for dyslipidemia. *Curr Opin Lipidol* 2017;**28**:193–200
59. Qian X, Hu J, Zhao J, Chen H. ATP citrate lyase expression is associated with advanced stage and prognosis in gastric adenocarcinoma. *Int J Clin Exp Med* 2015;**8**:7855–60
60. Zheng Y, Zhou Q, Zhao C, Li J, Yu Z, Zhu Q. ATP citrate lyase inhibitor triggers endoplasmic reticulum stress to induce hepatocellular carcinoma cell apoptosis via p-eIF2α/ATF4/CHOP axis. *J Cell Mol Med* 2021;**25**:1468–79
61. Chen Y, Li K, Gong D, Zhang J, Li Q, Zhao G, Lin P. ACLY: a biomarker of recurrence in breast cancer. *Pathol Res Pract* 2020;**216**:153076
62. Wen J, Min X, Shen M, Hua Q, Han Y, Zhao L, Liu L, Huang G, Liu J, Zhao X. ACLY facilitates colon cancer cell metastasis by CTNNB1. *J Exp Clin Cancer Res* 2019;**38**:401
63. De Magistris P. The great escape: mRNA export through the nuclear pore complex. *Int J Mol Sci* 2021;**22**:11767
64. Roussel M, Saule S, Lagrou C, Rommens C, Beug H, Graf T, Stehelin D. Three new types of viral oncogene of cellular origin specific for haematopoietic cell transformation. *Nature* 1979;**281**:452–5
65. Vennstrom B, Sheiness D, Zabielski J, Bishop JM. Isolation and characterization of c-myc, a cellular homolog of the oncogene (v-myc) of avian myelocytomatosis virus strain 29. *J Virol* 1982;**42**:773–9

(Received March 17, 2023, Accepted August 28, 2023)